Journal of Neuroscience Methods 172 (2008) 158–167

Contents lists available at ScienceDirect

Journal of Neuroscience Methods

journal homepage: www.elsevier.com/locate/jneumeth

A two-dimensional force sensor in the millinewton range for measuring vibrissal contacts

Brian W. Quist[a], Mitra J.Z. Hartmann[a,b,*]

[a] Biomedical Engineering Department, Northwestern University, 2145 Sheridan Road, Evanston, IL 60208, United States
[b] Mechanical Engineering Department, Northwestern University, 2145 Sheridan Road, Evanston, IL 60208, United States

ARTICLE INFO

Article history:
Received 12 December 2007
Received in revised form 12 March 2008
Accepted 14 March 2008

Keywords:
Force sensor
Contact sensor
Vibrissae
Whisker
Whisking

ABSTRACT

The rat vibrissal (whisker) array is a common model system in neuroscience used to study sensorimotor integration. Recent work has suggested that during object contact, the forces and moments at the whisker base may serve as important perceptual cues to the rat. To date, however, the force/moment profile that results from a whisker sweeping against an object has yet to be characterized, because it requires the simultaneous measurement of two-dimensional forces on the order of millinewtons. Current technology for these measurements typically involves prohibitively bulky, expensive equipment with complicated fabrication techniques. We have developed a simple, yet effective two-dimensional force sensor with ±0.02 mN resolution; it is extremely compact, has a highly linear static response with low-noise output, and is inexpensive to build. We demonstrate the advantages and limitations of the sensor in three different experimental protocols, ranging from the precise quantification of forces on isolated (plucked) whiskers, to the detection of whisker-contact times in the awake behaving animal. Given the high fidelity of the sensor, it could have utility in a broad range of applications in which measuring contact/detach occurrence and/or small magnitude forces are important.

1. Introduction

Rats have roughly 30 whiskers on each side of their face, each one exquisitely sensitive to tactile information. Using only tactual input to its whiskers, a rat can identify all of an object's spatial properties, including location, size, shape, orientation, and texture (Carvell and Simons, 1990, 1995; Brecht et al., 1997; Polley et al., 2005). We have recently demonstrated that moment at the whisker base can provide information about radial object distance, and hence is likely to be an important cue to the rat during object localization and discrimination behaviors (Birdwell et al., 2007; Solomon and Hartmann, 2006). This result is supported physiologically by the finding that some of the primary sensory neurons in the trigeminal ganglion encode radial distance as a function of whisker curvature (directly proportional to the moment) near the whisker base (Szwed et al., 2003, 2006). Despite the substantial evidence that the forces and moments generated during whisker/object contact are likely to serve as important perceptual cues to the rat, the force/moment profile as a whisker sweeps into an object has yet to be measured, due to the small magnitudes involved. We were motivated to construct a highly sensitive two-dimensional force sensor to quantify the contact forces that result from a rat vibrissa (whisker) sweeping against a point-object.

Current technologies for tracking a whisker's trajectory include optical techniques (Bermejo et al., 1998; Mehta et al., 2007) and contact detection (Bermejo and Zeigler, 2000). Optical techniques can successfully monitor whisker kinematics (i.e., position and its temporal derivatives), but cannot measure contact forces. Existing contact sensors use piezoelectric films and are limited to detecting contact/detach of the vibrissa with the sensor (Bermejo and Zeigler, 2000; Sachdev et al., 2001). In the present paper, we describe a force sensor that can be used to detect contact onset and offset as well as the continuous force/moment profile of a whisker in two dimensions. The sensor has low-noise and a highly repeatable output, while at the same time requiring a minimal amount of space to fit in experimental setups.

We first describe the sensor and quantify its frequency response curve. The functionality of the sensor is then demonstrated under tightly controlled experimental conditions in which an isolated (plucked) whisker is rotated at a known velocity into the sensor at two different radial distances. Under these controlled conditions, the sensor can be used to precisely quantify whisker forces in two dimensions. We then demonstrate the sensor's utility in three experimental protocols of gradually increasing complexity: during passive whisker stimulation in an anesthetized rat, during

* Corresponding author at: Mechanical Engineering Department, Northwestern University, 2145 Sheridan Road, Evanston, IL 60208, United States.
E-mail address: m-hartmann@northwestern.edu (M.J.Z. Hartmann).

0165-0270/$ – see front matter © 2008 Published by Elsevier B.V.
doi:10.1016/j.jneumeth.2008.03.004

artificial whisking, and during natural exploratory behavior of an awake, unrestrained rat. As the experiments increase in complexity, the sensor can no longer be used for precise force characterization, but rather offers a unique "window" into characterizing the whisking behavior of the rat. The sensor will likely find significance among researchers of the vibrissal, antennal, and cercal systems, and more general utility among researchers in any field measuring small magnitude forces.

2. Methods

2.1. Force sensor

As shown in Fig. 1a, the sensor was designed with three basic components: a Nitinol elastic wire, a pair of strain gauges, and a rigid base. The Nitinol wire was 0.025 in. in diameter (NW-025, Small Parts Inc.), and was rigidly connected at one end to the rigid steel base through the use of a cold-weld compound (8265-S, JB Weld). Nitinol was selected for its highly elastic properties, which enable the sensor to be extremely sensitive. The Nitinol wire was "sandwiched" between the pair of precision strain gauges (SG-3/350-LY11, Omega Engineering) close to the base, and fixed with an ethyl-based cyanoacrylate adhesive (Loctite 496, Omega Engineering). Forces applied anywhere along the length of the wire cause it to bend according to the principles of elasticity, which in turn compresses one of the strain gauges. The opposing strain gauge (on the opposite side of the wire) is elongated by an equivalent amount. Arranging the output of the two gauges in a Wheatstone half bridge configuration yields a circuit with an output sensitive to small displacements, yet resistant to environmental noise. Because both strain gauges experience virtually the same thermal events and common-mode noise, these unwanted components of the signal can be eliminated through the use of an instrumentation amplifier. All output was low-pass filtered in hardware at approximately 1500 Hz, and sampled at 3 kHz by a NI-DAQ board (NI-6059, National Instruments).

The second dimension of the sensor was added by placing a second pair of strain gauges directly above the first set of strain gauges on the wire (see Fig. 1a and b). Both gauges were attached in the same manner as described previously, but were rotated about the long axis of the wire by 90° to set them orthogonal to the first pair of strain gauges. In this way, we can detect wire displacements in two perpendicular coordinate directions. Construction was performed under a dissection microscope, and orthogonality of the strain gages evaluated by using a micrometer to displace the sensor tip in perpendicular directions while monitoring the voltage output of each pair. Errors in orthogonality are apparent as axis-crosstalk, and may be systematic enough to correct post-processing. Construction of the device is thus rather simple in comparison to other custom-built (Berkelman et al., 2003) or commercially-built sensor designs.

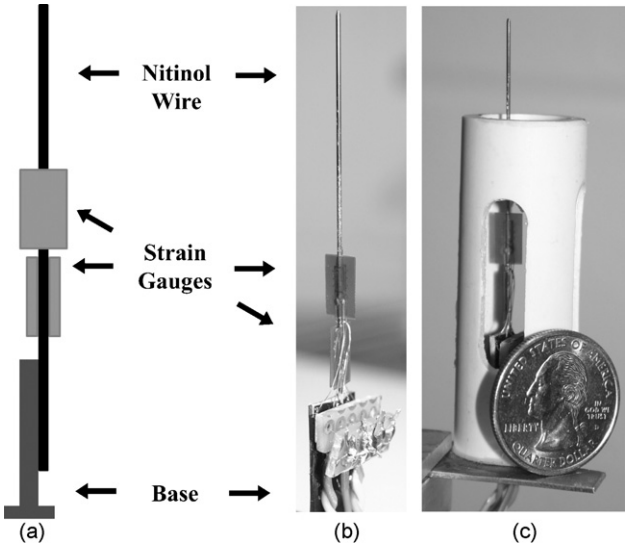

Fig. 1. (a) Schematic of 2D force sensor. The design is comprised of Nitinol wire, strain gauges, and the anchoring base. These are indicated by labeled arrows in both the schematic and (b) the photograph of the sensor. (c) Photograph of the sensor in its housing that removes small thermal drifts caused by ambient air currents. The windows assist the positioning of the sensor prior to experimentation. During data collection, the windows are covered using standard electrical tape. The quarter has been included for scale.

Because the second pair of strain gauges is mounted farther from the sensor base, their sensitivity to beam deflections is slightly smaller than the first. In addition, the leads from the second pair of strain gauges are more exposed. The output from this axis is therefore more susceptible to small convective air currents. To eliminate this thermal effect, a small (1/2 in. diameter) PVC pipe was fitted from the base of the sensor to approximately 2 cm above the top of the highest strain gauge (see Fig. 1c). The exact dimensions of the tube, however, can be altered to suit experimental needs, as any shape that creates a space of static-air around the sensor can perform the task. Windows were cut into the tubing to aid orienting the sensor prior to an experiment, but were covered using electrical tape before data collection began. Although simple, the tubing eliminated virtually all remaining thermal drifts to yield a sensor with a highly stable output, as will be shown in Section 3.

2.2. Sensor characterization: calibration, repeatability, and frequency response

Calibration of the sensor was performed gravimetrically. The correlation between force and sensor voltage output was obtained by hanging a series of weights from a point very close to the end of the sensor. The two axes of the sensor were calibrated independently, as follows: the sensor was first oriented horizontally to use gravity as a constant force to act on carefully weighed masses. The sensor was then rotated about its base in the horizontal plane to ensure that only one axis measured the deflection corresponding to the weight. For each trial, a baseline was measured and subtracted. A weight was then hung, and the sensor/weight system was allowed to come to rest. The difference between baseline voltage and the new voltage with the weight present was then calculated and saved. This was done 20 times for each weight, and for each axis. The weights used were 0.05 g, 0.1 g, 0.15 g, 0.2 g, and 0.3 g. During experiments, whiskers were rotated against the sensor at exactly the location where the weights had been hung. This ensured that the sensor output voltage was calibrated to provide an accurate measurement of whisker forces.

A precision micrometer (MP-285, Sutter Instrument Company) capable of 0.2 μm resolution was used to determine the repeatability of the sensor under a constant deflection. Before testing, the micrometer was brought to touch the sensor but induce no voltage change. Using a trapezoidal position profile, the micrometer then deflected the x-axis of the sensor 40 μm at a constant velocity of 3 mm/s (this represented the upper velocity limit of the micrometer) before returning to its original position. This was repeated 20 times. Without changing the orientation of the sensor, the micrometer was then positioned to displace 40 μm along the y-axis of the sensor. This too was repeated 20 times.

While these two previous tests provide a clear picture of how the sensor will behave quasi-statically, a complete picture of the sensor response includes a dynamic response test. Although the sensor itself will be fixed in place, the objects of interest (i.e., whiskers) have the potential to move quite rapidly. Greater whisk-

ing velocities, then, translate to larger impact forces into the sensor. This imparts an impulse to the sensor–whisker system that in theory excites all frequencies, and yields a detected output that can be distorted both in magnitude and phase directly dependent on the system response characteristics. We evaluated this frequency response of the sensor by constructing a custom testing apparatus. The core-component consisted of a 6.5" voice-coil speaker (WX-65X, Pyramid Car Audio). A custom-machined 2D sensor clamp was rigidly fixed to the speaker voice-coils, which permitted translation of the clamp in the direction of speaker motion. The 2D sensor was clamped to have its long axis perpendicular to the speaker translation direction. This allowed us to vibrate the sensor base by driving the speaker with a voltage waveform. The resulting position of the tip of the sensor was monitored by tracking its respective shadow across a 400 dots-per-inch linear sensor array (TSL1406R, Texas Advanced Optoelectronic Solutions Inc.). The highest sampling rate attainable for our sensor array was 645 Hz. In order to conservatively stay below the Nyquist frequency, we only drove the speaker up to 300 Hz. We generated the Bode diagram by sequentially driving the speaker at frequencies ranging between 2 Hz and 300 Hz, in 1 Hz increments. Data from the linear sensor array at each driving frequency was collected at both the tip and the base of the sensor; the resulting output was then processed to extract the sampled position. The particular response at each frequency was determined by digitally band-pass filtering the position signal at the driving frequency, and recursively fitting a sine-wave to the resulting filter output. The ratio of tip to base amplitude determined the magnitude response, while the difference in tip to base phase angle determined the phase diagram.

2.3. Sensor quantification using an isolated whisker

To evaluate the functional capabilities of the sensor, an individual whisker was plucked from the first column (arc) of the vibrissal array of an anesthetized Sprague–Dawley rat. The whisker was then attached to a DC motor equipped with an optical encoder (A-Max 32, Maxon Motors). The whisker was rigidly clamped to the motor using a washer and nut (Fig. 2a). Prior to running the test, the whisker was brought to just touch the sensor, but induce no voltage change in the sensor output. This angle was defined as 0°, and the axes of the sensor aligned to the direction of whisker movement. The motor was then programmed to follow a specific angular movement profile (denoted as $\theta(t)$ in Fig. 2b) defined by angular position, angular velocity and angular acceleration. Rotation of the whisker into the sensor resulted in a deflection of the sensor (denoted as $\vec{\delta}_\theta$ in Fig. 2b), detected by the sensor strain gauges. Under these highly controlled conditions, the whisker encounters the sensor perpendicular to its plane of rotation, and the whisker therefore tends not to slip along the length of the sensor (i.e., the whisker does not slip in and out of the page in Fig. 2b). A unique 2D force can thus be correlated with the change in sensor voltage (depicted as $\vec{F}_\theta$). This last step is performed offline in the post-processing phase of the experiment, and uses the relationship between force and sensor voltage output determined by the calibration method previously described.

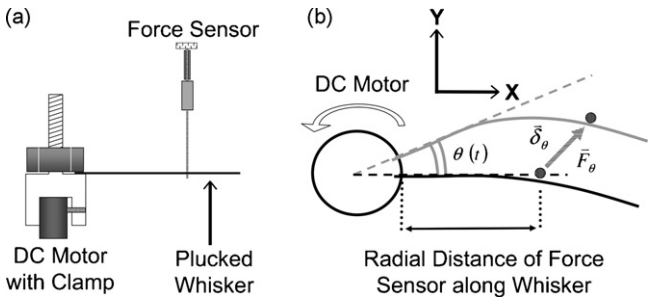

Fig. 2. Schematic of whisker force testing setup. (a) Side view of setup. A custom-built clamping device rigidly holds the plucked whisker in a fixed orientation. The clamping device is secured to a DC motor with an optical encoder. The sensor, inverted from the diagram in Fig. 1, is then placed at a specific radial distance from the whisker anchor point. (b) Top view of setup. Arrow above the DC motor indicates the direction of motor rotation. $\theta(t)$ denotes the difference in angle of rotation of the whisker from starting (black whisker) to a point in time, t, (shown as the grey whisker) beyond the sensor (depicted as the filled circle). The corresponding displacement, δ_Θ, at that angle is generated by a proportional force, F_Θ, due to the whisker.

The most straightforward use of the sensor is as a binary contact sensor. To demonstrate this utility, we rotated a plucked rat whisker that had been clamped in the mechanical setup (Fig. 2) into a single axis of the sensor. The mounted whisker was retracted to an initial motor encoder angle of −5°, where 0° is referenced as the angle at which the whisker touches the sensor but induces no voltage change. Next the motor moved the whisker at a slow rate of 50° s^{-1} in a trapezoidal position profile to an angle of +5°, before returning to the start position. We deliberately chose a slow velocity to avoid sensor dynamics (which had already been characterized as described above). Instead, the purpose of this experiment was to demonstrate the low force threshold required to generate a voltage change in our sensor. The trapezoidal position profile test was performed at two positions along the length of the whisker: one point was located 16% out along the whisker's length and the other point at 76% of the whisker's length. The two locations reveal how the interaction of an un-modified single whisker can trigger a detectable and significant voltage change. Acquired data from the single axis sensor was low-pass filtered at 70 Hz to remove minor sensor oscillations and DC motor electrical noise.

To evaluate the two-dimensional force profile of an idealized whisk that had a realistic amplitude and velocity, a whisker from the first column of the rat's vibrissal array was plucked and mounted with the sensor located at 50% along the length of the whisker. It was fixed in an orientation to closely match its natural orientation in the rat mystacial pad, and clamped with its convex side facing the sensor. A standard Cartesian coordinate system was used to quantify the direction of whisker forces, and was fixed throughout the duration of the trial. Fig. 2b illustrates this coordinate system in relation to the motor–whisker assembly as viewed from above. The whisker was then swept 20° into the sensor before being retracted back to its starting position. This was done using a rounded-trapezoidal position profile with constant velocity of 700° s^{-1}, which is close to the rat's protraction physiological average of 717 ± 186° s^{-1} (Jin et al., 2004). We chose this kinematic profile as a simple starting-point to investigate how 2D forces may vary over the course of a single idealized whisk. As will be further described in Section 4, there is no generic movement pattern for a whisk during natural exploratory behavior, and the rat has considerable control in changing this movement at any point during the whisk (Bermejo et al., 2002).

The raw output from the two-dimensional force sensor was then converted from a voltage to a force using the gravimetric calibration relationship described in Section 2.2. Finally, the signal was low-pass filtered at 70 Hz to remove the sensor resonance and DC motor electrical noise. These issues are further addressed in Section 4.2.

2.4. Sensor quantification using the intact vibrissal array

To evaluate the utility of the sensor in a wider variety of experimental situations, we used three experimental protocols. First, we used the sensor to record the force profile during passive displacement of a single whisker of an anesthetized rat. Second, we

stimulated the facial motor nerve (nVII) of an anesthetized rat to induce artificial whisking, and measured the force profile of a single whisker as it rotated into the sensor. Third, we placed the sensor in the whisking path of a freely behaving rat to determine whisker contact times. All procedures were approved in advance by Northwestern's Animal Care and Use Committee.

To test the sensor in passive displacement experiments, a Sprague–Dawley rat was anesthetized using a mixture of ketamine (75.8 mg/kg), xylazine (3.78 mg/kg), and acepromazine (0.76 mg/kg), and placed in a stereotaxic unit to fix the head position. The sensor was used in a protocol designed to imitate more controlled passive stimulation experiments, in which the whiskers are displaced known amounts by a precision controlled stimulator (Aguilar and Castro-Alamancos, 2005; Kwegyir-Afful and Keller, 2004; Li and Ebner, 2007; Minnery and Simons, 2003). For these experiments, the sensor was mounted on a linkage system positioned below the rat so that the sensor touched whisker C2 within the first third of the whisker's length. The axes of the sensor were oriented to match those seen in the clamped whisker setup (Fig. 2), with the *x*-axis aligned with the base of the whisker as it emerges from the follicle. The linkage system permitted a consistent orientation and smooth translation of the sensor in a horizontal plane below the rat. Displacement of the whisker was achieved by pivoting this linkage system by hand. High-speed video (Fastcam-512PCI, Photron) of whisker deflection was captured at 500 frames per second (fps) from a camera placed directly above the setup. Sensor voltage data was low-pass filtered in analog at approximately 1500 Hz, acquired at 40 kHz to facilitate synchronization with simultaneous neural recordings, and then low-pass filtered at 1500 Hz off-line. Both the video and sensor data acquisition were triggered and acquired simultaneously using LabVIEW. The whisker angle was tracked using custom-written MATLAB image processing software to analyze each frame of the movie offline, and was approximated using a line connecting a point near the base of the whisker to a point near the sensor contact region.

Next, we measured whisking forces generated during artificial whisking, induced by stimulation of the buccal branch of the facial motor nerve with a bipolar electrode (Szwed et al., 2003). The stimulation waveform was generated using an isolated pulse stimulator (Model 2100, A-M Systems), and was composed of a rectangular pulse with a current amplitude of 2.4 mA at a bursting frequency of 100 Hz. The experiment utilized the same rat as previously described for the controlled passive displacement with no changes to the positioning of the linkage system at whisker C2. This was done to permit a direct comparison between these two experimental paradigms. Whisking bouts into the sensor were captured with the same frame rates and camera trigger, and then processed to track the whisker angle as described above.

Finally, the sensor was placed in the whisking path of an awake, unrestrained, behaving rat. To motivate vigorous exploratory behavior, a Sprague–Dawley rat was placed in a novel environment on a balance beam. The sensor was placed within whisking-distance of the beam at a height intended to contact the lower half of the vibrissal array. Contact occurred during free-air exploratory whisking of the rat off the platform. All activity with the sensor was recorded using high-speed video from above at a frame rate of 500 fps. Sensor voltages were low-pass filtered at approximately 1500 Hz, acquired at 3 kHz, and synchronized off-line with the high-speed video.

3. Results

The goal of the present paper was to quantify sensor performance and demonstrate the sensor's utility in measuring vibrissal contact and forces under a variety of experimental conditions. A more comprehensive characterization of whisker force profiles is in progress (Quist and Hartmann, in preparation).

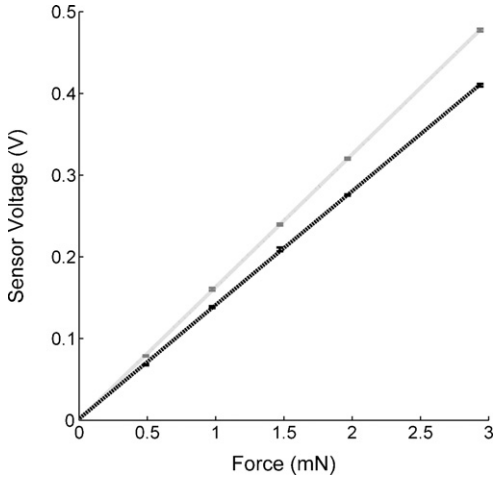

Fig. 3. Force–voltage calibration curve of the 2D sensor. Calibration points are shown with standard deviation error bars. Standard deviations are within the size of the data points. The dotted lines indicate the best-fit linear-regression line. The dark trace corresponds to the *x*-axis calibration curve of the sensor, while the grey trace corresponds to the *y*-axis calibration curve.

3.1. Sensor characterization: calibration, repeatability, and frequency response

The output of the calibration trials is shown in Fig. 3. Standard deviations are within the size of the data points. There was a strong linear relationship between weight and the sensor output. To quantify this relationship, linear regression was performed on the raw data to determine the slope and strength of the correlation (plotted as dotted lines). The adjusted R^2 value for the *x*-axis was found to be 0.9997, while the adjusted R^2 value for the *y*-axis was found to be 0.9999. From this data, the precision of the sensor could also be determined. A 95% confidence interval averaged across the calibration weights for any given *x*-axis reading was found to be $\pm$0.03 mN, while the corresponding 95% confidence interval for the *y*-axis was $\pm$0.02 mN. As described in Section 2.1, the two axes have slightly different sensitivities because the strain gages are mounted at slightly different distances from the base. Nevertheless, both our axes show a force sensitivity of $\pm$0.03 mN. This is better than can be done with most commercial sensors (see Section 4.1).

From the calibration analysis, it is expected that the standard deviation of the repeatability trials should be quite small. Indeed, it is clear in Fig. 4a and b that the sensor's output was so highly repeatable for such a small displacement as 40 μm that each trial plots nearly on the same line as the mean of the signal. Performing such a test using the precision micrometer can also reveal cases in which the two pairs of strain gauges are not properly set orthogonal to each other. Under these conditions, careful deflection of the sensor in only one dimension induces a change in voltage in the opposite axis. This type of mechanical crosstalk did not exceed 2% of the deflected axis voltage magnitude for either axis of our sensor.

The resulting frequency response of the sensor is shown in the form of a Bode magnitude plot (Fig. 5a) and Bode phase plot (Fig. 5b). The system is clearly underdamped, and exhibits a mechanical resonance frequency at approximately 120 Hz. Low frequency inputs below 20 Hz were faithfully transmitted by the sensor, indicating that quasi-static measurements of force and moment will be the most accurate. Noise in the Bode plot at high frequencies is likely

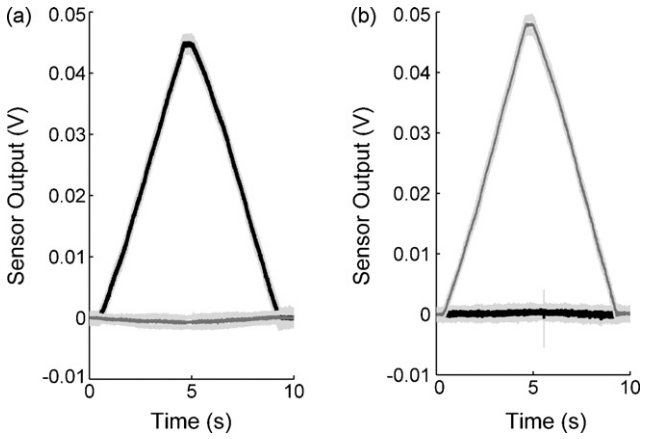

Fig. 4. Repeatability curves for the sensor. Each curve represents a mean of 20 repetitions of a 40 μm displacement of the (a) *x*-axis and the (b) *y*-axis. Sensor output from the *x*-axis is shown as black; the *y*-axis is shown in dark grey. The standard deviation for each channel is depicted in light grey.

due to errors in tracking the shadow of the rapidly moving 2D sensor by the linear sensor array.

3.2. Sensor quantification using an isolated whisker

One straightforward application of the sensor is as a highly sensitive binary contact detector to indicate times of whisker contact. The sensor can be used in this binary manner even when experimental conditions prohibit an accurate force–voltage calibration, for example when the whisker slips along the length of the sensor, or does not hit within the calibrated location of the sensor. Single-trial output for the locations 16% and 76% along the whisker's length are shown in Fig. 6a and b, respectively. The angular encoder output of the motor can be seen in Fig. 6c, in which the grey vertical lines signify the angular zero-crossings. The output of the sensor for both radial distances shows a strong correlation with the underlying motor rotation. Even at 76% of the whisker length, where forces reached a maximum of 0.024 mN, it is clear that the output closely matches the encoder angle. The sensor threshold is therefore most dependent on the baseline noise of the output, which can be quite low.

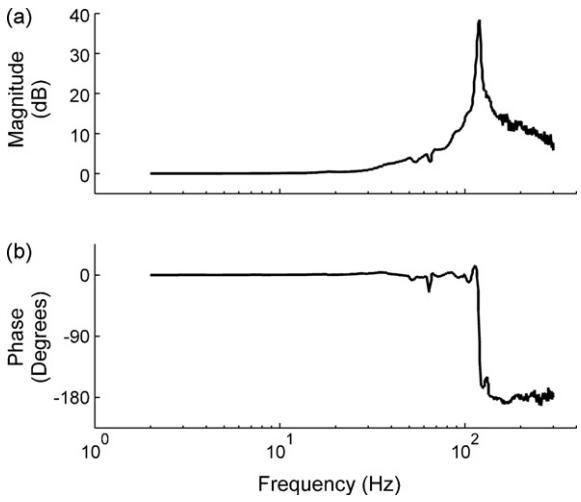

Fig. 5. Mechanical frequency response. (a) Bode magnitude plot and (b) Bode phase plot represent the mechanical resonance of the sensor, as determined by the relationship between the time dependent base position and the tip position.

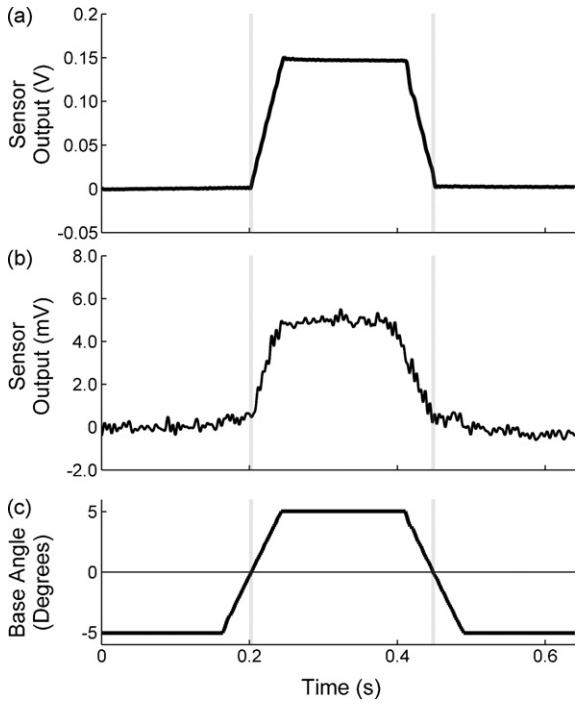

Fig. 6. Filtered output of a single axis of the 2D sensor for a motor base angle change of 5° is shown for a radial distance of (a) 16% of the whisker length and (b) 76% of the whisker length. The motor encoder angle as it varies with time is shown in (c). Grey vertical bars correspond to the encoder angle of 0°, which was calibrated as the whisker touching the sensor but inducing no voltage change.

It is important to note that the strong correlation between whisker deflection angle and force shown in Fig. 6 is not expected to occur when measuring whiskers remaining intact on the face of a rat. This is due to a whisking-associated mystacial pad movement that translates the base of the whisker (Bermejo et al., 2005), thus changing the relation between angle and force. Instead, the moments/forces measured by the sensor will represent the moments and forces occurring at the whisker base, regardless of whether the whisker is translated, rotated, or both.

In addition to its use as a binary contact detector, the sensor can also measure two-dimensional whisker forces. Conversion from sensor output to a force was done using the gravimetric calibration curves from Fig. 3, then low pass filtered as described in Section 2 to remove motor noise and sensor resonance. The final output reveals the two-dimensional time varying forces generated by the whisker as it is swept into and then is retracted from the sensor, as shown in Fig. 7. Both dimensions have unique features specific to the different phases of the mechanical "whisk." This suggests that forces in the two orthogonal directions could convey different information to the rat during the whisk cycle (Quist and Hartmann, in preparation).

The force profile of Fig. 7 before motor reversal is likely to accurately represent the force build up that would occur during a natural whisking protraction into an object. However, the effects seen in Fig. 7 after motor reversal are unlikely to represent the force profile during a natural retraction. The reason is that the increase in *x*-axis force during the mechanical "retraction" is likely to be the effect of a rigid boundary condition and fixed rotation point. One would expect any such effect for the real rat to be much less pronounced given the rat's likely ability to change the stiffness of the follicle complex (Rice et al., 1986) and the natural movement of the whisker rotational pivot point (Berg and Kleinfeld, 2003).

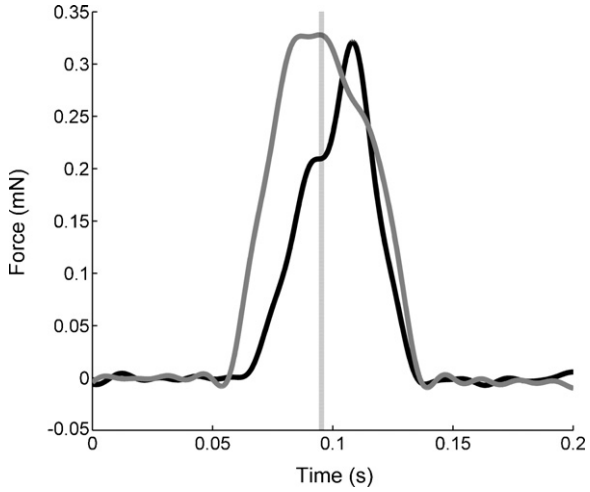

Fig. 7. Filtered 2D sensor output for a single trial of a whisker swept 20° into the sensor positioned at 50% along the whisker length. Force was calculated using the calibration curves of Fig. 3. Output from the sensor *x*-axis is shown in black, while the output from the sensor *y*-axis is shown in grey (consistent with Fig. 2). The vertical line indicates the time of motor rotation direction reversal.

3.3. Sensor quantification using the intact vibrissal array

The utility of the sensor is not limited to quantifying isolated whisker mechanics. We tested the sensor in three experimental protocols of increasing complexity: in passive whisker displacement experiments, in artificial whisking experiments, and finally, in experiments involving the awake, freely behaving rat.

To begin, we quantified the sensor's ability to measure force in a controlled passive stimulation experiment by displacing a large, caudal whisker of an anesthetized rat. Traditional passive displacement experiments use a precisely controlled stimulator to move a whisker with known amplitudes and velocities after its whisker-responsive neuron is found (Aguilar and Castro-Alamancos, 2005; Kwegyir-Afful and Keller, 2004; Li and Ebner, 2007; Minnery and Simons, 2003). With this experiment, we intended to use the sensor in a configuration that imitated this type of precisely controlled passive stimulation. Because we could control the height at which the whisker contacted the sensor, we could confidently measure contact forces. Raw output from the sensor was converted to force as described in Section 3.2, and low-pass filtered at 1500 Hz. The force output and tracked whisker angle are shown in Fig. 8a, while the accompanying video with force output of this trial can be seen in Supplementary Movie 1. As with the isolated whisker, there are clear differences in force profiles associated with each of the axes. Forces normal to the whisker (the *y*-axis, shown in dark grey) are in general larger than the forces along the whisker shaft (the *x*-axis, shown in light grey), and become negative at approximately 0.8 s into the trial because the whisker sticks to the sensor as it retracts. Because the sensor was primarily translated in the *y*-direction, there is good agreement between the *y*-axis force output and the tracked whisker angle. Despite this, a small error exists between these two traces that can be seen easily when observing the zero-crossing for the sensor angle and the *y*-axis force near 0.8 s into the trial, and is absent in Fig. 8b. Despite these small differences, the trial demonstrates that the sensor can be used as a force transducer during passive stimulation experiments, provided that the displacement mechanism is free of mechanical vibrations of its own.

The small differences between the *y*-axis force trace and the angle trace in Fig. 8a highlight an important point: namely, that the sensor can pick up subtle effects that are not evident from the video alone. In this experiment, the *y*-axis of the sensor indicates that there remains a force at the base of the whisker, even when the tracked-angle data would suggest that the force is zero. One reason for this discrepancy is that this experiment used an anesthetized rat whose mystacial pad was entirely relaxed. Displacement of the whisker therefore also resulted in displacing the follicle and supporting tissue to a point where it began to resist. This highly non-linear boundary condition means that the whisker may appear to emerge with an angle of "zero" even when significant forces near the base still exist.

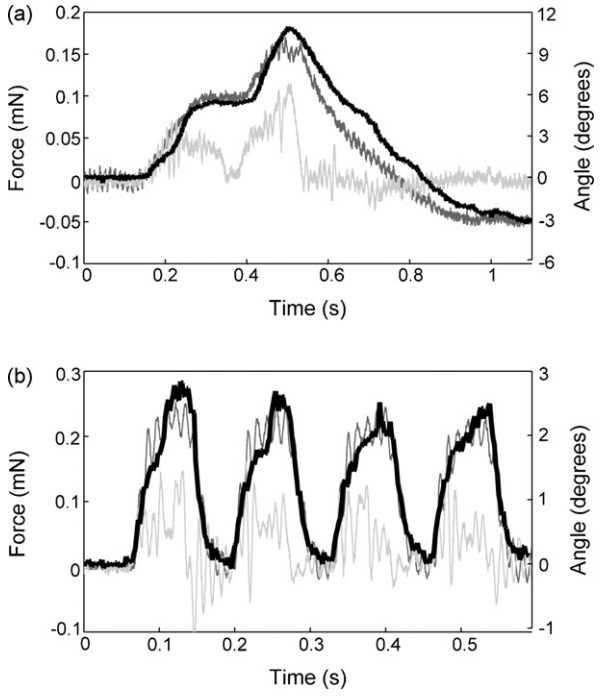

Fig. 8. 2D sensor output with video-tracked whisker position. (a) Passive displacement of the sensor into the whisker. Force output from the sensor for the *y*-axis (dark grey trace) and the *x*-axis (light grey trace) were computed using the calibration curves shown in Fig. 3, and are plotted on the left axis. Sensor axes were oriented to match Fig. 2. The corresponding whisker angle (black trace, plotted on the right axis) was acquired through image processing of the video. (b) Artificial whisking into the sensor. Force output and tracked whisker traces follow the color conventions established in (a).

Next, we used the sensor to measure the whisking force profile during artificial whisking. Artificial whisking does not replicate natural whisking, but serves as a complementary investigative tool to passive displacement experiments. Both the sensor data and video were processed in the same manner as for the passive displacement experiment, and are presented in Fig. 8b and Supplementary Movie 2. Artificial whisking produced an even stronger correlation between the sensor *y*-axis force (shown in dark grey) and the automatically tracked whisker angle (shown in black). This was true even though the contact point along the whisker remained the same as in the passive case. In addition, measured forces were larger than during passive displacement, despite a smaller total angular displacement (compare the right *y*-axes of Fig. 8a and b).

Two different vibration frequencies occurred during the artificial whisking and are each expected to elicit neural responses. The first frequency was introduced as a result of the periodic stimulation of the buccal nerve at 100 Hz, which induced strong periodic mystacial pad contractions. As a consequence, most vibrissae oscillated during their peak protraction (for example see frames 120–140 of Supplementary Movie 2). Szwed et al. (2003) found the neural response of their tonic cells were indeed locked to this stim-

ulation frequency. The second frequency was introduced as a result of resonance of the sensor at 85 Hz. Oscillations at this second frequency are clearly visible in the force sensor output as well as the tracked whisker angle (see Fig. 8b). Because the sensor's mass is large compared to the contacting vibrissae, it dominates the vibration response of the whisker–sensor system. Neural responses of that whisker follicle would therefore be expected to show 85 Hz modulations.

The utility of the sensor in precisely measuring force in this experimental setup is therefore diminished. Simply filtering out the resonant frequency of the sensor would be unfaithful to the corresponding neural responses. Also, the experimenter must ensure that the whisker hits the sensor at the calibrated location, and that only a single whisker interacts with the sensor. A modified sensor with a damper-backstop that prevents large negative *y*-axis oscillations could be used to gain a qualitative perspective on the moment profile occurring within the follicle of an artificially whisking rat.

Last, we tested the sensor's contact detection capabilities during the free exploratory behavior of an awake, unrestrained rat. To achieve this, the sensor was placed within the rat's whisking path as it explored off the end of a balance beam. In these types of natural conditions, the rat has considerable control over its whiskers; consequently, the vibrissal array generally moves in very different ways compared to either passive displacement or artificial whisking experiments.

For example, the rat can vary the position of the entire supporting mystacial pad (Berg and Kleinfeld, 2003; Wineski, 1985), which can occur in both the anterior–posterior and dorsal–ventral directions (Bermejo et al., 2005). The movement of individual whiskers cannot be simplified either. Each whisker moves through an ellipsoidal trajectory that can be altered during the whisk cycle (Bermejo et al., 2002). Individual whiskers can move divergently, as opposed to synchronously, as was once thought (Sachdev et al., 2002). Additional modulation of the whisker trajectories can occur when the awake, behaving rat interacts with an object. During object contact, the rat will often control its vibrissal array to make only light contact (Mitchinson et al., 2007).

In the present experiments, it did not make sense to convert sensor output to a measure of force, as a whisker could hit anywhere along the length of the sensor (far from the point that was calibrated), and multiple whiskers could hit the sensor. We therefore did not perform the calibration between force and voltage, as previously described, but only checked the orthogonality of the sensor axes. Instead, we used the sensor as a semi-quantitative "window" on rat behavior, and to capture whisker contacts that might otherwise have gone undetected. Although exact forces in this situation are no longer available, any forces acting on the sensor via the vibrissae still must have a reaction force within that whisker's follicle. The ability to estimate this is the "window" to which we refer. It reflects a qualitative insight derived from the direction and magnitude of sensor deflection into the whisker–sensor interaction that goes beyond the resolution capabilities of video or the output capabilities of a one-dimensional binary piezo sensor.

To process the signals, we first low-pass filtered the output from each axis at 80 Hz. This frequency was chosen by observing the power spectral density of the signals. The results for the *x*- and *y*-axis can be found in Fig. 9a and b, respectively. The axes are roughly equivalent to the orientation shown in Fig. 2 with respect to the whisker; however, this relation was not precise given the movement of the rat's head. Continuing, we then took the magnitude of the filtered output, which is simply the square root of the sum of the squares of each channel's output. This magnitude is shown in Fig. 9c as well as Supplementary Movie 3. Additionally, each frame was visually analyzed to serve as a reference

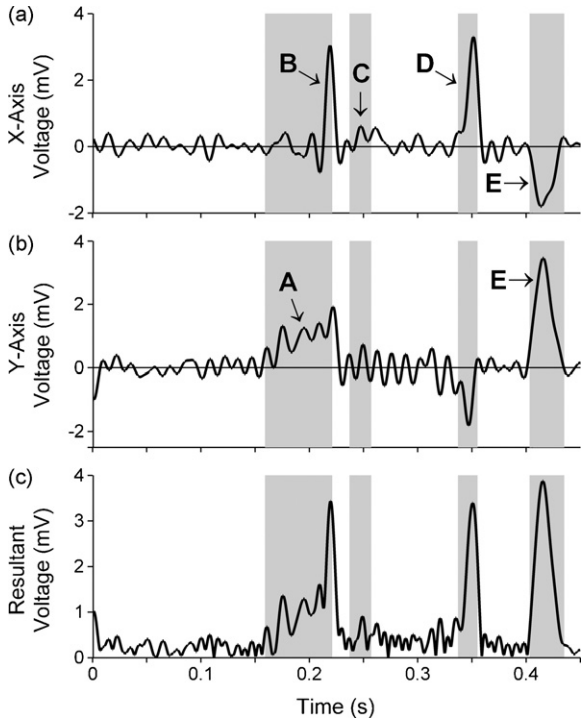

Fig. 9. Active whisking of a freely behaving rat into the 2D sensor. (a) Low-pass filtered *x*-axis sensor output versus time. (b) Low-pass filtered *y*-axis sensor output versus time. (c) Resultant voltage represents the square root of the sum of the filtered and squared voltage signals from each channel of the sensor. Grey vertical bar regions depict contact of the whisker with the sensor, as established by visually analyzing each frame offline. The first contact occurs with a whisker tip (A) and builds force gradually as the protraction progresses. The whisker tip becomes compressed at the beginning of retraction, resulting in a large upward spike in the *x*-direction force (B). The release is sudden, and causes the sensor to oscillate. Consequently, a more rostral whisker tip contact is not detected near the end of retraction (C). During the subsequent retraction, a whisker tip strikes the sensor and sweeps past (D). Finally, a pair of whiskers protract into the sensor (E).

for when vibrissae contact appeared to occur. The corresponding time associated with each "contact frame" appears in all subfigures of Fig. 9 as a series of grey vertical bars. Contact within these shaded bars occurred continuously, and did not contain any minor interrupts.

In the section of data shown, we can distinguish a rat's interaction with the sensor during protraction, retraction, and a slip-past of a whisker tip. The most complicated interaction of the three contact types we distinguish was with the whisker tip. In this situation, the sensor was much stiffer than the whisker. As a consequence, the forces built much more slowly and did not accurately indicate the precise time of contact (shown as arrow A in Fig. 9b). It is only until the tip was bent at a severe angle and retraction began that an easily discernable force developed (see arrow B in Fig. 9a). This large spike was the result of the whisker slipping along its length during protraction so that when the whisker movement direction reversed, the whisker tip could only compress. The tip sprang loose almost as soon as this occurred, which left the sensor to oscillate in free air. During that time, another whisker tip retracted into the sensor (see arrow C in Fig. 9a) but no signal could be detected because the sensor was not in a steady-state. For the next protraction, no contact occurred. Instead, it was during the retraction that a whisker tip struck the sensor (see arrow D in Fig. 9a). This resulted in a sudden compression along the whisker shaft. Finally, a number of whiskers from the array protracted into the sensor and provided a strong signal to both the *x*- and *y*-axis (see arrow E of Fig. 9a and b).

4. Discussion

We have demonstrated a simple yet effective technology for the measurement of millinewton forces in two dimensions. The sensor has output that is both highly linear and repeatable. It was specifically developed to measure forces due to vibrissal contact, and could replace the piezoelectric sensors currently in use as contact sensors in laboratories that study the electrophysiology and behavior of the vibrissal system. In addition, given its sensitivity to such small forces, the device also has the potential to be used in more standard engineering applications.

4.1. Comparison to current sensor technology

Force sensors come in a variety of designs as diverse as the applications in which they are used. When selecting a sensor that can measure millinewton forces in more than one dimension simultaneously, however, this selection pool becomes much smaller. Custom-built multi-dimensional force sensors often combine sets of strain gauges, as can be seen in the work of Berkelman et al. (2003). Their device involved constructing a miniature sensor to be mounted on the end of microsurgical instruments, with miniature strain gauges mounted to thin elastic beams arranged radially about a central sensing tip. The design can measure forces in three dimensions, with a filtered signal resolution of 0.49 mN. Two-axis sensing using orthogonal sets of strain gauges has also been implemented by Wilson and Chen (1995), but only to measure position. Their design employed a long steel wire with shim steel soldered to the base of the wire; strain gauges were then affixed to these pieces of steel in a similar configuration as we have described. The "whisker" apparatus was then actuated with pneumatic tubing, and was used successfully to determine the contour of certain objects. No specifics regarding force were investigated given that their primary goal was contour extraction.

When evaluating multi-axis sensors, no commercial products were functionally capable of monitoring whisker interactions given their size, resolution, or mounting constraints. Only the custom-built sensors that used strain gauges appeared to match our criteria. The device of Berkelman et al. (2003) was indeed sensitive, but was also complicated to fabricate since it required electrical discharge machining. The more simplistic design of Wilson and Chen (1995) looked promising, but a characterization of the sensor's capabilities was not provided in their findings. In the end, we chose a design modified from that of Wilson and Chen, with highly effective results and performance characteristics comparable to other multi-axis sensors.

The utility of our sensor compared to current sensor technology depends on the application for which it will be used. Given the relative cost and simplistic construction for our sensor, it may be surprising to see that our technology is equivalent or better than many commercial load cells and force transducers. The material cost alone for our device is roughly 5% of the cost for off-the-shelf comparable commercially available products. In specific comparison to a BIOPAC 50 g force transducer (BIOPAC Systems Inc., Goleta, CA) in our laboratory, we have found that our sensor is superior in terms of susceptibility to electrical noise, and has no measurable thermal drift. Furthermore, we have demonstrated linearity correlation coefficients of nearly one, with repeatability trials yielding error bars that are difficult to distinguish from the mean for such small displacements as 40 μm.

Given the sensor's small size, it can be readily incorporated into experimental setups with a minimal impact on space. This cannot always be said of other sensing technologies. Commercial products specifically available from Tetra (Ilmenau, Germany), which use a glass-spring with fiber optics to monitor the displacement, can offer high precision force resolution down to 0.02 mN for the their 100 mN sensor. It is interesting to note our sensor demonstrated a comparable resolution, which was 0.02 mN and 0.03 mN for the *x*-and *y*-axis, respectively. Whereas the Tetra systems are designed for studies in tribology and require a specific testing apparatus, our sensor can theoretically be placed almost anywhere. With respect to the 3D force sensor of Berkelman et al. (2003), our sensor is limited to measure forces in two dimensions; however, we have demonstrated force resolution capabilities for our sensor that are an order of magnitude smaller than the 3D sensor.

4.2. Addressing limitations of the sensor

One of the primary concerns when determining whether to use this sensor in a particular application is the tendency for the sensor to resonate when impacted. This behavior can affect both the ability to accurately measure forces as well as binary contact times.

The resonance of the sensor can be attributed to the sensor acting as a cantilever beam with a rigid boundary condition at its fixed end. These oscillations in the output can commonly occur in two instances. The first is if the vibrissa (or other object rotating into the sensor) has slipped off the sensor while still displacing the sensor tip, and the free-end of the sensor is then allowed to come to a steady-state. Oscillations will occur at the free-end of the sensor, but will negligibly affect the system being investigated. An example of this type of oscillation is seen in Supplementary Movie 3, where one of the awake rat's whiskers flicks past the sensor. The second instance of oscillations will occur when the object that initially deflects the sensor subsequently starts to follow the dynamics of the sensor. For example, in Supplementary Movie 2, the whisker initially deflects the sensor, but as it continues to protract, its movements are then entrained to the sensor resonance. Ideally, the resonant frequency of the sensor can be clearly separated from the input frequencies of relevance; a notch-filter can then effectively remove the unwanted oscillation frequencies.

These resonant oscillations may be of concern when using the sensor during electrophysiology experiments measuring vibrissae force in an anesthetized or head-fixed rat. It has been shown previously that receptors in the follicle can respond to frequencies as high as 1 kHz (Gibson and Welker, 1983; Gottschaldt et al., 1973), and ganglion neurons at least up to 300 Hz (Moore and Andermann, 2005). Given that the resonant frequency of the sensor is well within this range, oscillations from the sensor could add an unwanted mechanical input to drive neural activity. The resonant oscillations might be reduced by providing a back-stop to arrest post-contact oscillations. In a similar fashion, the susceptibility of the sensor to oscillate during contact detection can be minimized by ringing, but not touching, the wire mid-height with a circular rubber-stopper to decrease the available deformation space.

4.3. Measuring forces versus moments with a cantilever beam or with a rat whisker

Have we constructed a force sensor, or have we constructed a moment sensor? This question gets at the heart of how strain-gauge-based commercial load cells and force sensors – and presumably how rat whiskers – operate. A force can be directly measured only if it is directly applied to a sensing element such as a strain gage or a biological mechanoreceptor. If the force is applied some distance away from the sensing element (e.g., transmitted through a lever arm), then the sensing element will experience both a moment and a force. The moment will be equal

to the cross product between the lever arm length, L, and the force, F. The moment is a measure of the sensing element's resistance to rotation, while the force is a measure of its resistance to translation. If the force is applied at any significant distance away from the sensing element, the moment, rather than the force, will strongly dominate its mechanical deformation. Thus, the sensor described in the present publication might be most accurately labeled as a "moment" sensor. The force can be accurately calculated, however, as long as the distance L is known. This is the same way that many commercial load cells operate (see Section 4.1).

For our application, we have ensured that the location of the object displacing the sensor occurs at the same radial distance along the wire close to its tip. In addition, we assume that the deflection of the tip is relatively small, which ensures that that force acting on the sensor will be orthogonal to the long axis of the wire. Implicit here, as well, is that the force is acting normal to the wire; this condition is ensured when initially setting up the sensor. When these conditions are satisfied, our results clearly show that the resulting sensor output is highly linear for the range of forces applied (Fig. 3). A similar method of using a cantilever beam to measure force through deflection can be found in the work of Albert et al. (2001), who used pulled glass fibers (capillaries). These authors measured beam deflection optically via a microscope, whereas our sensor measures the deflection using precision strain gauges. In both instances, the radial distance of contact is carefully noted.

It is interesting to note that the rat would face a similar challenge in determining the magnitude of force acting on one of its whiskers. We predict that deformation of mechanoreceptors in the follicle will be strongly dominated by their resistance to rotation, rather than translation, and that they will therefore be more sensitive to bending moments than to forces. An exception may be the force directed longitudinally along the whisker, which, as shown in Fig. 7, can be quite significant. In previous publications, we have suggested that the rat combines such information about moment with information about the whisker's velocity (either translational, rotational, or combined) to determine the radial distance L at which the whisker hit an object.

Measuring the forces exerted by moving whiskers on the sensor raises yet another question: what fraction of the measured force is attributable to the whisker-sensor collision force, and what fraction is attributable to post-contact bending of the whisker? We expect collision forces to be quite small for a number of reasons: first, the whisker mass is extremely small relative to the objects it will likely encounter; second, the taper of the whisker reduces the mass closer to the tip where contacts are more likely to occur; third, the elasticity of the whisker will increase the time duration over which the velocity change takes place, effectively decreasing the impulse to the sensor. This suggests that nearly the entire measured force will be a result of bending forces of the whisker. In addition to bending forces, damping is also likely to have a significant effect (Hartmann et al., 2003).

Finally, the question of whether a collision force exists is linked to a more general question: can a whisker be treated as a massless spring? The results of the present study suggest – but do not prove – that damping forces plus bending forces together dominate inertial forces. Any rotational inertial effect will also depend strongly on boundary conditions at the follicle. The inertial effects are expected to be smaller when the whisker is held by a real follicle than when it is rigidly clamped at the base. The softer base of the follicle will reduce the mechanical ability of the whisker to be elastically spring loaded, effectively decreasing momentum transfer.

In conclusion, we have presented a two-dimensional force sensor with high-resolution, low-noise, and highly linear and repeatable output. The sensor is extremely versatile given its size and cost, and should find use in a wide range of applications measuring small-scale forces and contacts.

Acknowledgements

This work was supported by an NSF graduate research fellowship to BWQ and NSF award IOB-0446391 and IIS-0613568 to MJZH. We thank Ed Colgate and Matt Tresch for useful advice on characterizing the sensor.

Appendix A. Supplementary data

Supplementary data associated with this article can be found, in the online version, at doi:10.1016/j.jneumeth.2008.03.004.

References

Aguilar JR, Castro-Alamancos MA. Spatiotemporal gating of sensory inputs in thalamus during quiescent and activated states. J Neurosci 2005;25:10990–1002.
Albert JT, Friedrich OC, Dechant HE, Barth FG. Arthropod touch reception: spider hair sensilla as rapid touch detectors. J Comp Physiol A 2001;187:303–12.
Berg RW, Kleinfeld D. Rhythmic whisking by rat: retraction as well as protraction of the vibrissae is under active muscular control. J Neurophysiol 2003;89:104–17.
Berkelman PJ, Whitcomb LL, Taylor RH, Jensen P. A miniature microsurgical instrument tip force sensor for enhanced force feedback during robot-assisted manipulation. IEEE Trans Robot Autom 2003;19:917–22.
Bermejo R, Zeigler HP. Real-time" monitoring of vibrissa contacts during rodent whisking. Somatosens Mot Res 2000;17:373–7.
Bermejo R, Houben D, Zeigler HP. Optoelectronic monitoring of individual whisker movements in rats. J Neurosci Methods 1998;83:89–96.
Bermejo R, Vyas A, Zeigler HP. Topography of rodent whisking. I. Two-dimensional monitoring of whisker movements. Somatosens Mot Res 2002;19:341–6.
Bermejo R, Friedman W, Zeigler HP. Topography of whisking II: interaction of whisker and pad. Somatosens Mot Res 2005;22:213–20.
Birdwell JA, Solomon JH, Thajchayapong M, Taylor MA, Cheely M, Towal RB, et al. Biomechanical models for radial distance determination by the rat vibrissal system. J Neurophysiol 2007;98:2439–55.
Brecht M, Preilowski B, Merzenich MM. Functional architecture of the mystacial vibrissae. Behav Brain Res 1997;84:81–97.
Carvell GE, Simons DJ. Biometric analyses of vibrissal tactile discrimination in the rat. J Neurosci 1990;10:2638–48.
Carvell GE, Simons DJ. Task-Related and Subject-Related Differences in Sensorimotor Behavior During Active Touch. Somatosensory Motor Res 1995;12:1–9.
Gibson JM, Welker WI. Quantitative studies of stimulus coding in 1st-order vibrissa afferents of rats 2. Adaptation and coding of stimulus parameters. Somatosens Res 1983;1:95–117.
Gottschaldt KM, Iggo A, Young DW. Functional characteristics of mechanoreceptors in sinus hair follicles of cat. J Physiol Lond 1973;235:287–315.
Hartmann MJ, Johnson NJ, Towal RB, Assad C. Mechanical characteristics of rat vibrissae: resonant frequencies and damping in isolated whiskers and in the awake behaving animal. J Neurosci 2003;23:6510–9.
Jin TE, Witzemann V, Brecht M. Fiber types of the intrinsic whisker muscle and whisking behavior. J Neurosci 2004;24:3386–93.
Kwegyir-Afful EE, Keller A. Response properties of whisker-related neurons in rat second somatosensory cortex. J Neurophysiol 2004;92:2083–92.
Li L, Ebner FF. Cortical modulation of spatial and angular tuning maps in the rat thalamus. J Neurosci 2007;27:167–79.
Mehta SB, Whitmer D, Figueroa R, Williams BA, Kleinfeld D. Active spatial perception in the vibrissa scanning sensorimotor system. Plos Biol 2007;5:309–22.
Minnery BS, Simons DJ. Response properties of whisker-associated trigeminothalamic neurons in rat nucleus principalis. J Neurophysiol 2003;89:40–56.
Mitchinson B, Martin CJ, Grant RA, Prescott TJ. Feedback control in active sensing: rat exploratory whisking is modulated by environmental contact. Proc R Soc B: Biol Sci 2007;274:1035–41.
Moore CI, Andermann ML, editors. The vibrissa resonance hypothesis Nashville. Tennessee: CRC Press; 2005.
Polley DB, Rickert JL, Frostig RD. Whisker-based discrimination of object orientation determined with a rapid training paradigm. Neurobiol Learn Mem 2005;83:134–42.
Rice FL, Mance A, Munger BL. A comparative light microscopic analysis of the sensory innervation of the Mystacial pad. 1. Innervation of vibrissal follicle-sinus complexes. J Comp Neurol 1986;252:154–74.

Sachdev RNS, Sellien H, Ebner F. Temporal organization of multi-whisker contact in rats. Somatosens Mot Res 2001;18:91–100.
Sachdev RNS, Sato T, Ebner FF. Divergent movement of adjacent whiskers. J Neurophysiol 2002;87:1440–8.
Solomon JH, Hartmann MJ. Robotic whiskers used to sense features. Nature 2006;443:525.
Szwed M, Bagdasarian K, Ahissar E. Encoding of vibrissal active touch. Neuron 2003;40:621–30.
Szwed M, Bagdasarian K, Blumenfeld B, Barak O, Derdikman D, Ahissar E. Responses of trigeminal ganglion neurons to the radial distance of contact during active vibrissal touch. J Neurophysiol 2006;95:791–802.
Wilson JF, Chen ZH. A whisker probe system for shape perception of solids. J Dyn Syst Meas Cont Trans Asme 1995;117:104–8.
Wineski LE. Facial morphology and vibrissal movement in the golden-hamster. J Morphol 1985;183:199–217.